metals

MDPI

Article

Hybrid Structures Made of Polyurethane/Graphene Nanocomposite Foams Embedded within Aluminum Open-Cell Foam

Susana C. Pinto [1], Paula A. A. P. Marques [1], Romeu Vicente [2], Luís Godinho [3] and Isabel Duarte [1,*]

1 Department of Mechanical Engineering, TEMA, University of Aveiro, 3810-193 Aveiro, Portugal; scpinto@ua.pt (S.C.P.); paulam@ua.pt (P.A.A.P.M.)
2 Department of Civil Engineering, RISCO, University of Aveiro, 3810-193 Aveiro, Portugal; romvic@ua.pt
3 Department of Civil Engineering, ISISE, University of Coimbra, 3030-788 Coimbra, Portugal; lgodinho@dec.uc.pt
* Correspondence: isabel.duarte@ua.pt; Tel.: +350-234-370-830

Received: 15 May 2020; Accepted: 5 June 2020; Published: 9 June 2020

Abstract: This paper focuses on the development of hybrid structures containing two different classes of porous materials, nanocomposite foams made of polyurethane combined with graphene-based materials, and aluminum open-cell foams (Al-OC). Prior to the hybrid structures preparation, the nanocomposite foam formulation was optimized. The optimization consisted of studying the effect of the addition of graphene oxide (GO) and graphene nanoplatelets (GNPs) at different loadings (1.0, 2.5 and 5.0 wt%) during the polyurethane foam (PUF) formation, and their effect on the final nanocomposite properties. Globally, the results showed enhanced mechanical, acoustic and fire-retardant properties of the PUF nanocomposites when compared with pristine PUF. In a later step, the hybrid structure was prepared by embedding the Al-OC foam with the optimized nanocomposite formulation (prepared with 2.5 wt% of GNPs (PUF/GNPs2.5)). The process of filling the pores of the Al-OC was successfully achieved, with the resulting hybrid structure retaining low thermal conductivity values, around 0.038 $W \cdot m^{-1} \cdot K^{-1}$, and presenting an improved sound absorption coefficient, especially for mid to high frequencies, with respect to the individual foams. Furthermore, the new hybrid structure also displayed better mechanical properties (the stress corresponding to 10% of deformation was improved in more than 10 and 1.3 times comparatively to PUF/GNPs2.5 and Al-OC, respectively).

Keywords: open-cell foam; polyurethane foam; hybrid structures; graphene-based materials; nanocomposites

1. Introduction

In recent years, porous materials have attracted a huge interest from both academia and industry because they may find applications in a variety of fields, such as energy storage [1], catalysis [2], drug release [3], sound and thermal insulation [4], environmental remediation [5] and others. Giving the International Union of Pure and Applied Chemistry (IUPAC) definition, porous materials can be categorized based on their pore sizes: microporous (pore size <2 nm), mesoporous (2–50 nm), and macroporous (>50 nm) [6]. According to these categories, the properties of the porous materials and their subsequent applications will differ. Moreover, they can be found in three-dimensional (3D) and two-dimensional (2D) structures. Common 3D porous materials are sponges, foams, wood, and bone. Two-dimensional porous materials include separation membranes, filter paper, textiles, and so on.

Depending on the previously referred characteristics, and additionally based on their chemical composition, the porous materials can present multifunctionality. Multifunctional materials offer multiple characteristics that can be translated into excellent performance in existing applications and also open up avenues for untouched application fields [7]. These can exist naturally or can be engineered, with the latter being usually obtained by combining two or more materials. New functionalities arise from the synergistic combination of the individual materials properties [8].

One interesting example of porous materials are aluminum open-cell foams (Al-OC). This type of foam is characterized by a low weight, high thermal and electrical conductivities, and high internal surface area. Furthermore, they are recyclable and non-flammable [9]. However, they present a low compressive strength, when compared, for example, with closed pore cell foams. To overcome this drawback, Al-OC foams can be combined with other materials, such as silicone [10,11], epoxy [10,12], or polyurethane [13]. Although the mechanical performance of the composite foams is compensated, their final weight is increased, which is not desirable for certain applications requiring lightweight structures. In this context, filling these metallic skeletons with lightweight porous materials can be an interesting alternative to bulk polymers. Reinfried M. et al. [14] explored the concept of hybrid foams, which consist of two different interpenetrating embedded foam-material classes. The idea behind the hybrid foams is to overcome the individual shortcomings of single-material foams by combining foams of two different material classes and therefore achieving synergistic property combinations that are relevant and beneficial for future applications.

Recently, our research group explored the concept of lightweight multifunctional hybrid structures by combining Al-OC foams with cellulose/graphene foams [15]. We reported the impregnation of a cellulose/graphene foam into an Al-OC foam, creating a hybrid structure with higher mechanical properties (increase in stress of 100 times) with respect to the cellulose foam. This multifunctional hybrid foam presented also high sound absorption coefficient (near 1 between 1000–4000 Hz) and low thermal conductivity.

To further explore these types of structures, in the present work we considered the incorporation of polyurethane foams (PUF) into Al-OC ones. PUF are known for their excellent thermal and acoustic insulation properties, low thermal conductivity, good mechanical and chemical stability and low manufacturing cost [16]. The PUF represents three quarters of the production of polyurethane (PU) materials and the major market sectors include insulation materials in buildings, shock absorbers for vehicles, packaging, footwear, and furniture [17,18]. However, due to their high flammability, the improvement of their fire-retardancy properties became crucial [19]. Taking this into account, PUF precursors like polyols have been synthetized with specific chemical functional groups to confer fire retardancy [16,20]. In addition, nanoclays (montmorillonite) [21], titanium dioxide [22], iron oxide magnetic nanoparticles [23], expandable graphite [19,24], and carbon nanostructures [25–29] have also been employed to confer flame retardancy. Often, the combinations of different fillers are used to access improved fire-retardancy behavior due to a synergetic effect [30,31]. Interestingly, the graphene-based materials' addition to polymeric matrices has been reported to provide, besides fire-retardancy, the ability to improve the mechanical properties [32,33] and sound absorption features [34,35].

Pursuing the goal to contribute to the development of lightweight multifunctional materials, this work presents, in a first step, the effect of the addition of two graphene-based materials, graphene oxide (GO) and graphene nanoplatelets (GNPs) on the PUF properties. The focus was on the fire retardancy, mechanical, acoustic, and thermal properties. After the characterization of the different PUF nanocomposites, a selected composition was incorporated in an Al-OC, creating a lightweight multifunctional hybrid structure that was further characterized.

2. Materials and Methods

2.1. Materials

The raw materials employed in PUF synthesis were: (i) methylene diphenyl diisocyanate (MDI) (VORANATE M229 from Dow Chemicals, Estarreja, Portugal), with average functionality of 2.7 and NCO content of 31.1%; and (ii) polyol, with a hydroxyl value of 239 mg KOH/g (VORACOR CR1112 from Dow Chemicals, Estarreja, Portugal).

Graphene oxide (GO) (4 mg/mL aqueous dispersion) was purchased from Graphenea (San Sebastián, Spain) and graphene nanoplatelets (GNPs) in powder were acquired from Cheaptubes (Cambridgeport, MA, USA). Silicone oil was acquired from Sigma-Aldrich (Darmstadt, Germany). The AlSi7Mg0.3 open-cell foams with pore sizes of 10 ppi (pores per inch) were supplied by Mayser GmbH & Co. KG (Lindenberg, Germany).

2.2. Sample Preparation

Pristine PUF and PUF nanocomposites were prepared by a two-step procedure, as schematized in Figure 1, route A. First, the pre-polymer (polyol), silicone oil (5 wt%), water as blowing agent (5 wt%) and GO or GNPs (1.0, 2.5 and 5.0 wt%) were placed in glass beaker and homogenized for 30 s using a mechanical stirrer at high speed. Next, the proper amount of MDI to obtain a $R_{NCO/OH}$ = 0.80 (ratio between NCO groups of isocyanates and OH groups) was added and the mixture was homogenized again for 10 s. The PUF and PUF nanocomposites were obtained by free expansion in the cup mold at room temperature. The foams are hereafter referred as PUF, PUF/xGNPs and PUF/xGO, where x refers to the carbon nanostructure content.

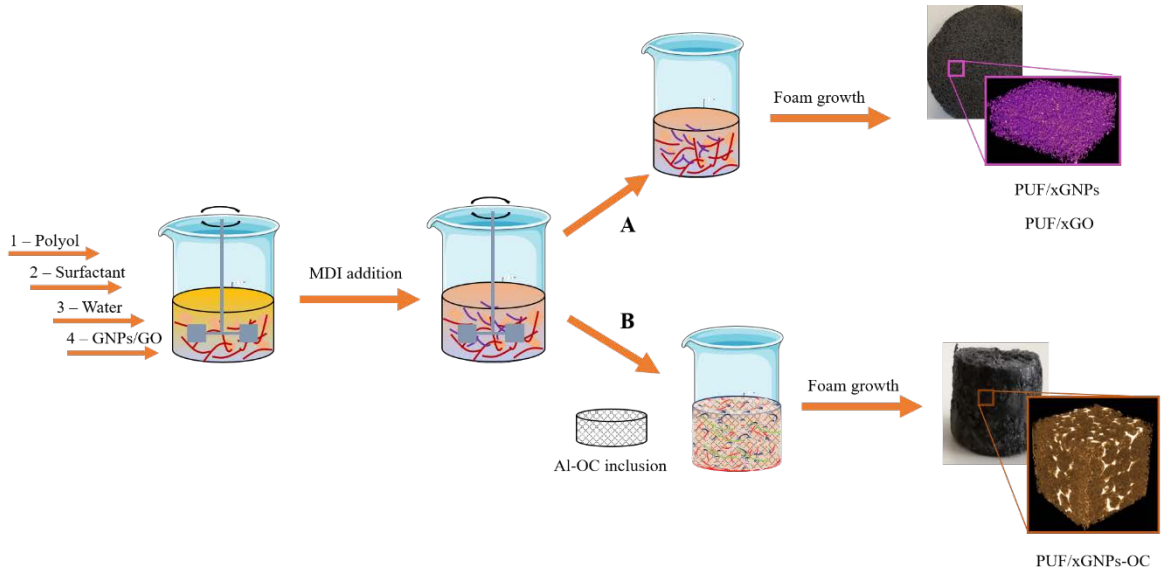

Figure 1. Scheme describing the preparation of: (**A**) polyurethane foam (PUF) nanocomposites; and (**B**) hybrid structures.

For the preparation of the Al-OC hybrid (the interconnected porous metallic foam with the optimized PUF nanocomposite) the metallic foam was placed into the cup containing the nanocomposite mixture right after the addition of MDI. The pores of the Al-OC were filled during the nanocomposite foam expansion (Figure 1, route B), hereafter referred as PUF/GNPs2.5-OC. Before characterization, the samples were settled to rest for 24 h at room temperature to ensure complete reaction.

2.3. Sample Characterization

Attenuated total reflection–Fourier transformed infrared spectroscopy (ATR-FTIR) spectra were collected using a Perkin Elmer FTIR System Spectrum BX Spectrometer (Buckinghamshire, UK) equipped with a single horizontal Golden Gate ATR cell, in the range 4000 to 500 cm^{-1} and running 64 scans with a resolution of 4 cm^{-1}. Scanning electron microscopy (SEM) analysis was performed in a TM 4000 Plus (Hitachi, Tokyo, Japan) scanning electron microscope at accelerating voltage of 15.0 kV. Samples ($10 \times 10 \times 10$ mm^3) were analyzed in a X-ray microcomputed tomography (μCT) equipment from SkyScan 1275 (Bruker μCT, Kontich, Belgium) with penetrative X-rays of 30 kV and 125 μA, in high-resolution mode with a pixel size of 8 μm and 450 ms of exposure time. NRecon and CTVox software (Bruker, Kontich, Belgium) were used for 3D reconstruction and CTan software (Bruker, Kontich, Belgium) was used in morphometric analysis (total porosity, pore size distribution and cell-wall thickness). The apparent density and porosity were determined geometrically for three specimens of each PUF nanocomposite.

The thermal conductivity properties were evaluated with a Hot Disk TPS 2500 S instrument (Gothenburg, Sweden), at 20 °C; in accordance with the standard ISO 22007-2.2 and ASTM D7984, the specimens were cube shaped with ($25 \times 25 \times 25$ mm^3). The value of the sound absorption coefficient was estimated from measurements made with an impedance tube according standard ASTM E 1050 [36] for cylindrical shaped specimens with 37 mm of diameter and 22 mm of thickness. The thermal stability of the nanocomposites foams was assessed by thermogravimetric analysis (TGA) using a thermogravimetric analyzer (Netzsch Jupiter, Selb, Germany) at a scanning rate of 10 °C/min, in the temperature range of 30–800 °C, under a synthetic air atmosphere (80% N_2 and 20% O_2). The fire retardancy test was based in the direct observation of the response of the specimens when submitted to a flame. The test consisted in applying an ethanol flame, at the specimen's bottom using the set-up in vertical sample position, for 3 s, plus a subsequent application (3 s) if the specimen self-extinguished. The tests were conducted in half cylindrical shaped specimens, with 30 mm of diameter and 10 mm of thickness.

The mechanical testing machine (Shimadzu MMT, Kyoto, Japan; maximum load 101 N) was used to study the quasi-static compressive response of PUF nanocomposites ($10 \times 10 \times 10$ mm^3) under a strain rate of 1 mm/min up. The uniaxial compression test of Al-OCF and hybrid PUF structures were performed in a Shimadzu-AGS-X-10kN (Kyoto, Japan) testing machine at a speed of 6 mm/min.

3. Results

3.1. PUFs Nanocomposites

The success of PUF and PUF nanocomposites preparation relies on the appropriate reaction between the precursors, namely the extinction of isocyanate groups through the reaction with hydroxyl groups of the polyol and urethane formation; this was confirmed by FTIR analysis (Figure S1). The addition of GO or GNP, at the used concentrations, did not prevent the progression of foam formation. However, the GO and GNPs did not disperse in the same way in the polymer matrix, as can be easily observed in the left column of Figure 2. The photographs show a homogeneous black color when GNPs were added, suggesting a good interaction between these nanofillers and the polymer matrix. On the contrary, black spots were observed in the PUF when the GO was used. The GO nanosheets were directly obtained from the chemical exfoliation of graphite and contain several oxygen chemical functionalities, which is what makes the GO highly hydrophilic. The GNPs were also obtained from graphite exfoliation, but without the use of chemical oxidants, thus resulting in a non-oxidized surface [37], GNPs being hydrophobic. This difference in the chemical surface structure of the carbon nanostructures determines their dispersion in the polymeric matrix, which have hydrophobic domains enabling GNPs dispersion. This section will provide a concise and precise description of the experimental results, their interpretation, as well as the experimental conclusions that can be drawn.

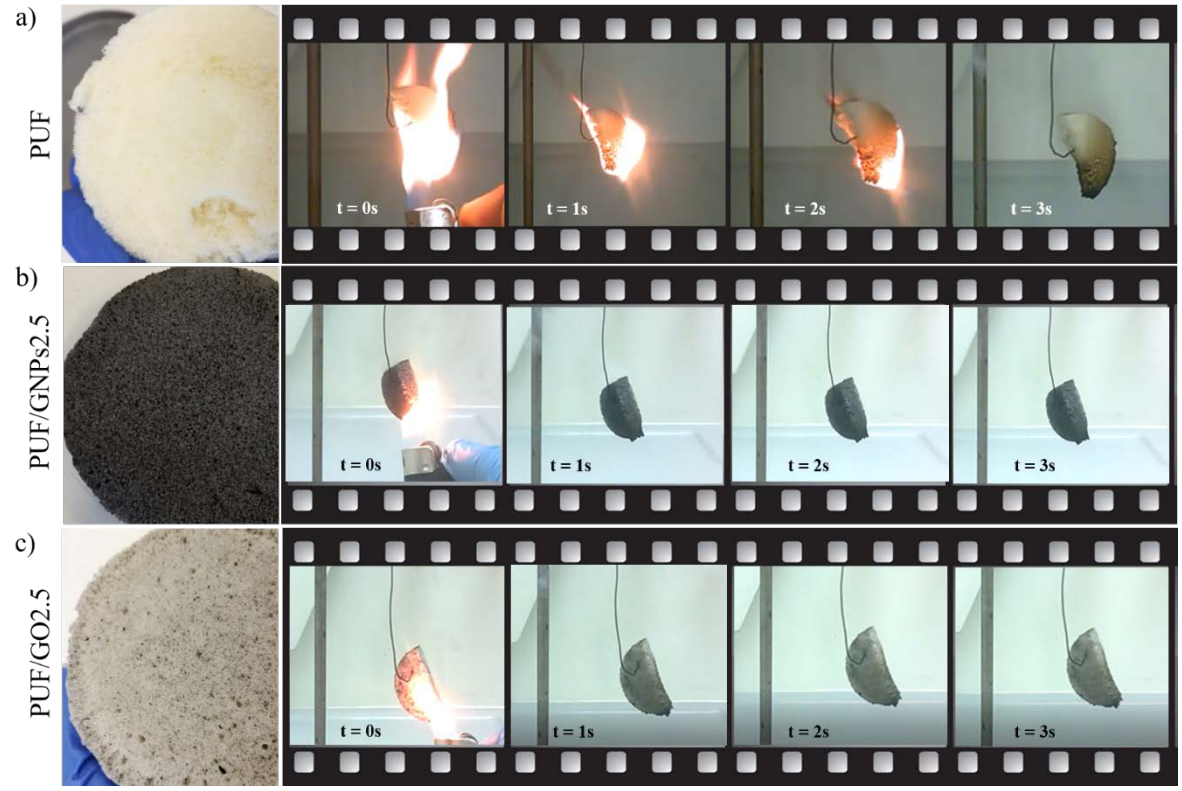

Figure 2. Flame behavior of: (**a**) PUF, (**b**) PUF/GNPs2.5, and (**c**) PUF/GO2.5.

3.1.1. Thermal Stability

Although the dispersion of both nanofillers (GNPs and GO) was not the same, their flame-retardant action was remarkable. A control test with pristine PUF showed flame propagation at some extension with smoke release, even if no dripping was observed, (Figure 2a). On the contrary, PUF nanocomposites prepared with 2.5 wt%, showed fire retardant properties, with the flame extinguished after 1 s. Importantly, the specimens maintained their shape after burning without dripping or smoke release (Figure 2b,c). Similar behavior was observed for the compositions with 5.0 wt% of the GO or GNPs. For the lower nanofillers amount tested (1 wt%), the results were not as good, since at 3 s there was still flame propagation, mainly for PUF/GNPs1.0, with smoke release in both cases (Figure S2). Carbon nanostructures are known to play a key role either in slowing down the flame propagation or even in providing self-extinction to thermoplastic or thermosetting polymeric matrices [38]. Their positive effect in the thermal stability of PUF nanocomposites may be attributed to the high specific area and layered structure of the nanofillers, which tend to form a dense and continuous char layer acting like a physical barrier at the PUF surface. This barrier becomes an obstacle to the release of the volatile degradation products, preventing or causing the delay of the degradation of the whole composite [39]. It is remarkable that, although the GO nanosheets are not as good dispersed as the GNPs in the polymer foam (photographs in the left side of Figure 2b,c), their effect on the flame retardancy was as efficient or even more efficient than the GNPs. GO's benefits in the fire retardancy efficacy over graphene have been referred to and are attributed to the GO oxygen functionalities that decompose and dehydrate at quite low temperatures. This causes a cool down of the polymer substrate during the combustion process and simultaneously release gaseous species that dilute the oxygen atmosphere near the ignition zone [30,39,40]. Graphene and GO are described mainly as co-flame retardants, at loadings from 1.0 to 10 wt% [41]. Also, functionalized graphene designed and prepared from expandable graphite and phosphorus-containing compounds has been described as flame retardants and smoke suppressor of PUF at 6.1 wt% [30]. It is worth mentioning that in our study, the pristine PUF and PUF nanocomposites with 1 wt% of nanofillers also kept their shape after burning. However, due to the

better results obtained for 2.5 and 5.0 wt%, the PUF with 1.0 wt% of nanofillers were excluded in the further characterization results.

The thermogravimetric (TG) and derivative thermogravimetric (DTG) curves are shown in Figure S3a,b, respectively. The pristine PUF and PUF nanocomposites showed similar TGA curves, suggesting that GNPs and GO do not significantly influence the decomposition of PUF. This finding is most likely related to the small amount of nanofillers used. The initial decomposition temperature corresponding to 5% ($T_{5\%}$), and 50% ($T_{50\%}$) of mass degradation, the maximum-rate degradation temperature (T_{max}), and mass residue at 750 °C are listed in Table 1. The results show that GNPs had a positive effect on $T_{5\%}$ on PUF, while GO was detrimental to the early thermal stability. These results are caused by the earlier degradation of the GO oxygen functionalities at low temperature, thus accelerating the degradation of the PUF matrix. The oxygen functionalities of GO may interact with the PUF precursors during the foam formation thus interfering with the crosslinking reaction, as reported by Gama et al. [19]. In fact, at high temperatures there is the complete burning of GO, proved by the lower percentage of residue at 750 °C [42]. The sample PUF/GNPs2.5 presents the higher thermal stability with $T_{50\%}$ of 404 °C. It was reported by Liu et al. [43] that graphene can act as a heat source and accelerate the decomposition of PUF. As so, the 2.5 wt% seems to have a more positive effect on the thermal properties of PUF than 5.0 wt%.

Table 1. Experimental data of TGA analysis.

Samples	$T_{5\%}$ (°C)	$T_{50\%}$ (°C)	T_{max} (°C)	Residue 750 °C (%)
PUF	173.6	349.8	312.3	5.68
PUF/GNPs2.5	197.7	404.6	314.7	5.18
PUF/GNPs5.0	188.5	392.9	316.5	5.12
PUF/GO2.5	165.4	360.7	311.4	2.42
PUF/GO5.0	149.2	355.6	312.9	1.88

3.1.2. Morphology

SEM images of pristine PUF and PUF nanocomposites show an inhomogeneous open-cell structure composed by quasi-spherical interconnected pores for all specimens. However, depending on the presence or absence of nanofillers, some small differences were noticed. As shown in Figure 3a insets, the GNPs and GO sheets are located, and sometimes wrapped, in the PUF cell walls. It is reported that carbon nanostructures have a nucleating effect during foam formation, thus altering the PUF morphology [44]. Usually, the presence of such fillers decreases the average cell size and increase foam density improving damping properties, flame-retardancy, and mechanical properties [45]. By comparing PUF/xGNPs with PUF/xGO SEM images, GO seems to promote thicker cell walls and joints which can be related with the agglomeration of GO or from the affinity of polyol and MDI with GO. The GO nanosheets are located between adjacent cavities of the foam, and the cell wall sticks together around them, producing thicker cell walls. This effect is accentuated with the increase in the quantity of GO: PUF/GO5.0 presented bigger pore size and thicker cell walls than PUF/GO2.5. On the contrary, the increase of GNP content in the PUF promotes a pore size decrease.

The 3D reconstruction performed by μCT analysis (Figure 3b) confirms the high porosity of the specimens, with porosity values of 94.4% for PUF, 93.8% for PUF/GNPs2.5, 93.5% for PUF/GO2.5, 91.9% for PU/GNPs5.0, and 91.8% for PUF/GO5.0. The μCT images also demonstrated that the morphology of the samples is heterogeneous with wide range of pore size and wall thickness. The mean cell sizes for pristine PUF, PUF/GNPS2.5, PUF/GO2.5, and PUF/GNPs5.0 are in the range 168–328 μm, while for PUF/GO5.0 these are located between 328–468 μm (Figure 3c). PUF/GO5.0 nanocomposites have also higher percentage of thicker wall cells (Figure 3d). It is worth mentioning that, due to the limitation of resolution of μCT, only pores and cell walls thickness above 8 μm were detected.

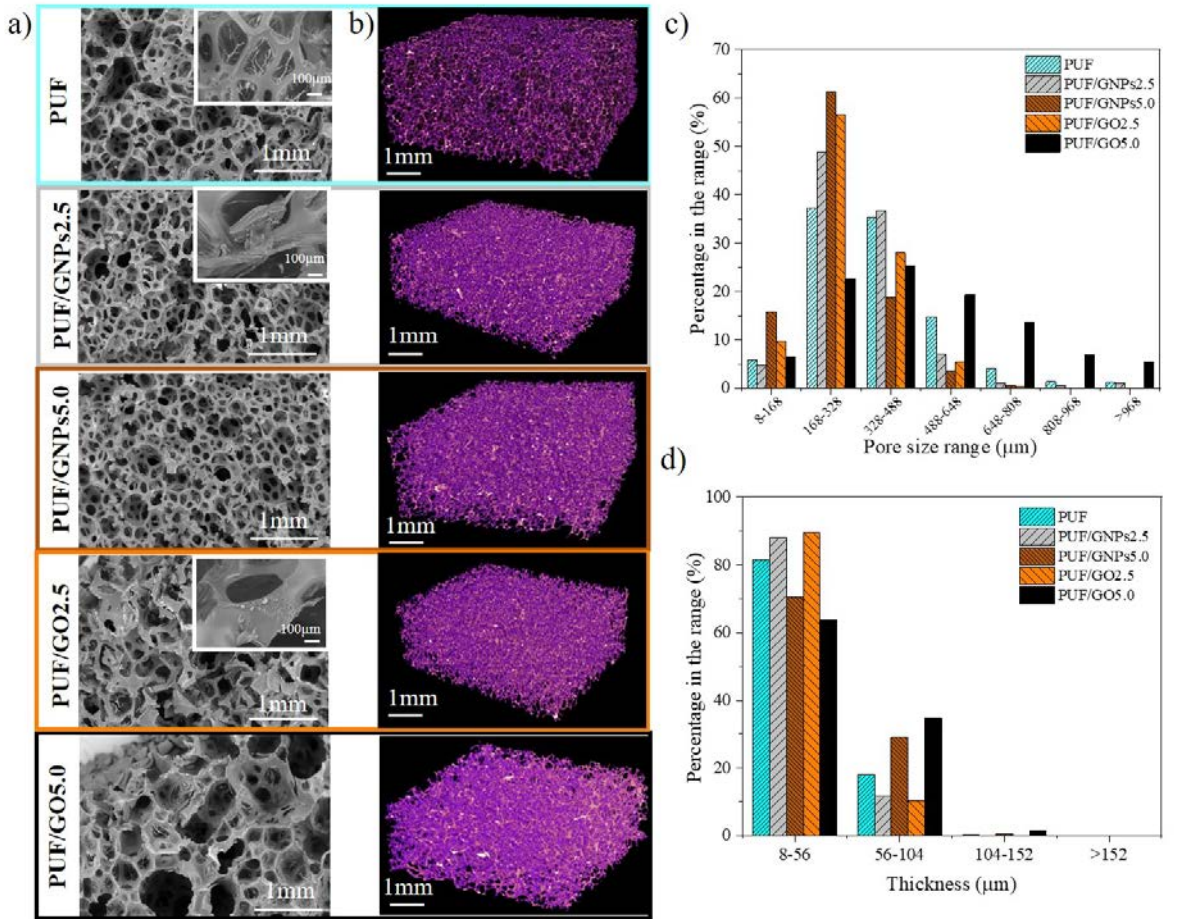

Figure 3. (**a**) SEM images, (**b**) 3D μCT rendering, (**c**) pore size distribution, and (**d**) cell wall thickness distribution for PUF, PUF/GNPs2.5, PUF/GNPs2.5, PUF/GO2.5, and PUF/GO5.0.

3.1.3. Mechanical Properties

The mechanical properties of the foams, the apparent density, the compressive strength at 10% of compression, and the compressive modulus are summarized in Table 2. The results indicate that the foams' densities increase with either GO and GNPs loading. In addition, the compressive strengths and compressive modulus steadily grow with the increase of both nanofillers content. It is reported that the addition of nanofillers to cellular materials can have different effects depending on several aspects, the loading content, the size and shape, the compatibility between the nanofillers and the matrix [33,46]. For the same fillers loading, the GO provides higher compressive modulus and higher resistivity to undergo load without total collapse of pores (higher stress plateau) than the GNPs. From the SEM images it was observed that GO induced thicker cell walls, while PUF/GNPs were similar to PUF. The improvement of compressive modulus and strength by the addition of carbon nanostructures to PUF was also reported by other experimental works, where phosphorus-functionalized GO [30] and expandable graphite [19] were used. Furthermore, MDI has isocyanate terminal groups (NCO) that can react with carboxylic and hydroxyl groups of GO leading to the chemical cross-linking between GO and PU matrix via the formation of amides or carbamate esters, thus improving the mechanical response [47].

From the average stress–strain compressive curves (Figure 4a), the foams exhibit the typical behavior of cellular materials. An elastic region at low strain values (5% of strain), where the stress–strain curve is linear, followed by a near constant stress until 55–60% of strain, is designated the stress plateau. Finally, densification takes place, with the complete collapse of the cells and the formation of a compact material, like a thin film, which is characterized by an abrupt increase of stress.

Table 2. Apparent density, compressive modulus, and compressive strength for 10% of deformation (n = 5).

Samples	Apparent Density (kg/m^3)		Compressive Modulus (kPa)		Compressive Strength (kPa) (Strain: 0.1)	
	Mean Value	Standard Deviation	Mean Value	Standard Deviation	Mean Value	Standard Deviation
PUF	44	1.1	247	3.6	21.7	0.7
PUF/GNPs2.5	47	0.8	570	12.8	28.3	5.8
PUF/GNPs5.0	56	2.0	966	81.9	48.3	5.4
PUF/GO2.5	50	1.2	598	46.4	35.3	0.3
PUF/GO5.0	60	3.6	1510	165.4	56.3	5.0

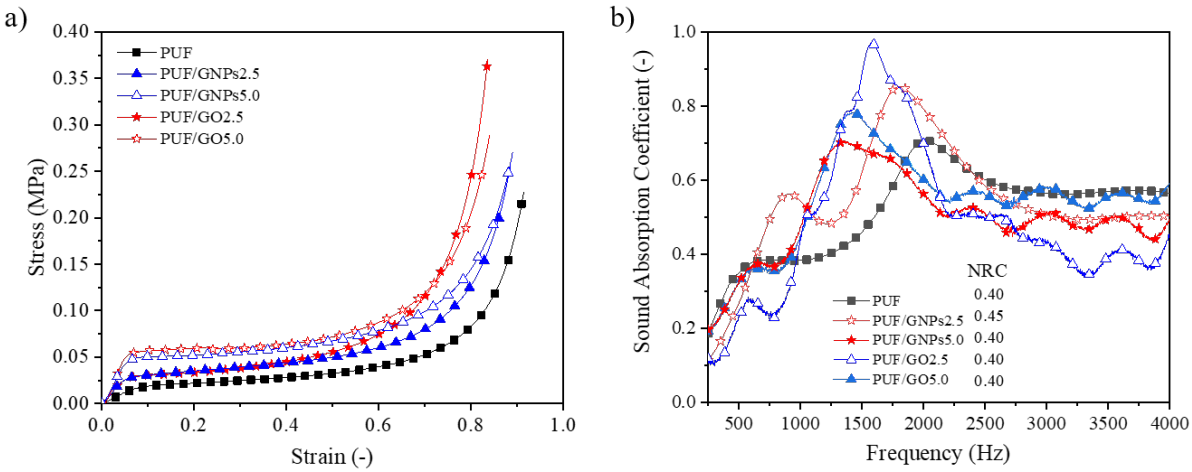

Figure 4. (**a**) Average stress–strain compressive curves; (**b**) the sound absorption coefficient of the different PU based composite foams.

3.1.4. Sound Absorption

Figure 4b shows the sound absorption coefficient between 100 and 4000 Hz for the PUF and PUF with 2.5 and 5.0 wt% of GNPs and GO. Globally, the sound absorption coefficient increases with frequency until 1500 Hz, followed by a small decrease and finally a subsequent stabilization between 2000 and 4000 Hz. The sound absorption coefficient is strongly influenced by the morphology of the foams, namely the density (associated to cell-wall thickness) and pore features (size, quantity, interconnectivity, tortuosity) [48]. It was reported that a smaller interconnected pore structure gives a better sound absorption coefficient due to the high airflow resistivity provided by cell walls [49]. Furthermore, higher porosity, associated with low density offers less resistance to sound-wave dissipation which results in a low sound absorption coefficient. Many factors contribute or influence the sound absorption, and therefore the overall values are a balance of all factors [17,48,50,51]. The incorporation of GNPs and GO increases the compressive modulus (with the later presenting higher values), and thus the cells have greater propension to undergo cell stretching, bending, and buckling without deformation. Also, by SEM and μCT analysis it was observed that the incorporation of GNPs and GO fillers decreases the porosity and pore size. The PUF/GO2.5 has the higher sound absorption curve between 1250 and 1750 Hz, reaching the value of 1 and absorbing more than approximately 50% than PUF. In fact, between 1000 and 1750 Hz, all the PUF nanocomposites have superior sound absorption coefficient comparatively to pristine PUF, which covers the sensitive frequency region of the human ear [34]. One parameter often used to describe sound absorption is the noise reduction coefficient (NRC). This parameter corresponds to the average of the sound absorption coefficients at the octave bands of 250, 500, 1000, and 2000 Hz, and rounding the result to the nearest multiple of

0.05. However, the use of NRC has its limitations since equal NRC values do not necessarily translate the same curve profile. Thus, it is worthwhile to use all the available data, especially for sound absorption at frequencies below 250 Hz or above 2000 Hz. The NRC values are gathered in Figure 4b and results showed that, although PU/GO2.5 and PU/GO5.0 have the same NRC that PU/GNPs5.0, they have distinct profiles of sound absorption vs. frequency, in this case, with PU/GO2.5 having better performance between 1200–2000 Hz. Gama et al. [17] obtained similar NRC values around 0.40–0.45 for PUF with a similar density (around 40 kg/m^3) and a higher thickness (approximately 40 mm).

3.1.5. Thermal Conductivity

To evaluate the possible application of these types of foams as thermal insulation materials, their thermal conductivity was evaluated (Table 3). A good thermal insulation material should present low thermal conductivity. The results obtained for all specimens (0.035–0.037 W·m^{-1}·K^{-1}) are in the range of most widely used commercial insulation materials, 0.030–0.040 W·m^{-1}·K^{-1} as reported in the literature [18,52,53]. The thermal diffusivity decreases with the addition of carbon nanostructures, except for the PUF/GO5.0, as listed on Table 3. This could be due to the barrier effect created by the nanofillers that difficult the heat flow.

Table 3. Thermal conductivity, thermal diffusivity, and specific heat (n = 5).

Samples	Thermal Conductivity (W·m^{-1}·K^{-1})		Thermal Diffusivity (mm^2·s^{-1})		Specific Heat (MJ·m^{-3}·K^{-1})	
	Mean Value	Standard Deviation	Mean Value	Standard Deviation	Mean Value	Standard Deviation
PUF	0.0352	0.0004	0.8577	0.0065	0.0410	0.0003
PUF/GNPs2.5	0.0361	0.0001	0.8037	0.0004	0.0448	0.0001
PUF/GNPs5.0	0.0393	0.0002	0.7672	0.0119	0.0486	0.0010
PUF/GO2.5	0.0355	0.0001	0.8276	0.0060	0.0429	0.0003
PUF/GO5.0	0.0366	0.0001	1.001	0.0060	0.0360	0.0002

From the combination of different materials, it was expected to create different multifunctional structures with high strength and reduced weight as a result of the synergetic effect of the individual materials which could be applied in different fields. In this sense, following the characterization of PUF nanocomposites regarding their fire retardancy, mechanic, acoustic, and thermal insulator properties, the formulation PUF/GNPs2.5 was selected to be incorporated in the Al-OC skeleton as a filling material and denoted as PU/GNPs2.5-OC. However, it is worth mentioning that all the developed PUF nanocomposites were suitable to be incorporated inside Al-OC.

3.2. Hybrid Structures

The effect of filling the voids of Al-OC foams with bulky polymers has been reported [10–12,54], showing enhanced mechanical properties due to the pore filling which improves the compressive strength and energy absorption capacity of the hybrid foams. However, the use of bulky polymers to fill the voids of the Al-OC foams can be disadvantageous when lightweight structures are required. Here, we wanted to explore the properties of the hybrid structure resulting from filling the Al-OC foam with a porous one, thus not compromising the lightness of the final structure. An easy and simple process to prepare this hybrid was followed (Figure 1, route B).

3.2.1. Structure

Figure 5a,b show the Al-OC and the PU/GNPs2.5-OC photographs, respectively, and in Figure 5c a 3D reconstruction of the hybrid structure obtained by μCT analysis is presented. It is worth mentioning that the weight ratio of Al-OC and PUF/GNPs 2.5 in the hybrid structure was 48.2% and

51.8%, respectively. It was observed that, during the PUF nanocomposite expansion, when in contact with Al-OC structs, some of the foam cells started to collapse. Because of that, the PUF/GNPs2.5 structure inside the Al-OC foam presented a different porosity and morphology from the optimized one. Although the pores were not uniform and the control of the porosity during the foaming was not possible, it ensured that the procedure were performed under the same operating conditions. In addition, the hybrid structures were reproducible as a whole, taking into account not only the filling material but the also the Al-OC. Though no chemical bonding between the metal surface and polymer was observed or even expected, an excellent form-fitting connection of the PUF/GNPs2.5 to the rough metal surface was visible by direct observation. The PUF/GNPs2.5 density was increased in the vicinity of the metal surface, visible in the color scheme (green color, Figure 5c).

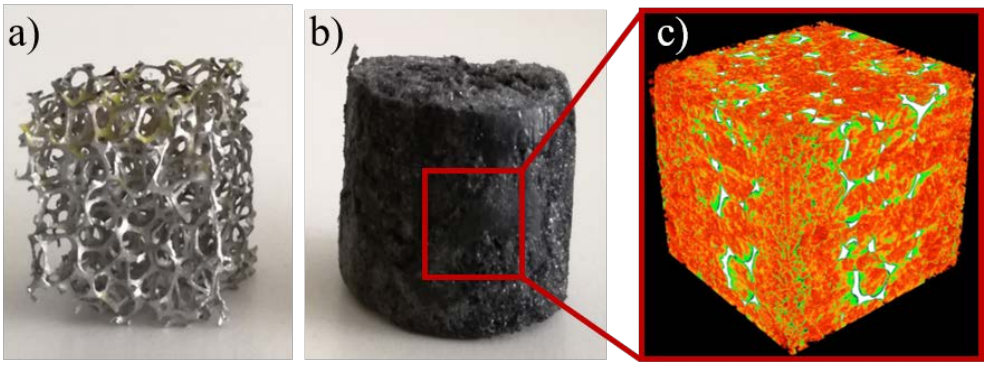

Figure 5. Specimens (**a**) Al-OC; (**b**) PUF/GNPs2.5-OC; and (**c**) μCT PUF/GNPs2.5-OC.

3.2.2. Mechanical Properties

The stress–strain curve is shown in Figure 6a and the energy absorption (EAD) and specific energy absorption (SEA) are illustrated in Figure S4. As described earlier for pristine PUF and PUF nanocomposites, these hybrid structures also present the typical behavior of foams, with three distinct regions: elastic, stress plateau, and densification [10]. Comparing the PU/GNPs2.5-OC compressive response with Al-OC, a similar behavior can be observed; however, with higher stress peak and stress plateau values and the densification occurring earlier. The EAD is higher for hybrid structures, with improvements of 27% comparative to the Al-OC foam and 13 times lower than the PUF/GNPs2.5. However, the SEA is lower, suggesting that the increase in EAD does not compensate the increase in weight, as found by Reinfried [14], that combined a steel open-cell foam with an expanded polystyrene foam. The values of apparent density, stress peak, EAD and SEA, and thermal conductivity are gathered in Table 4.

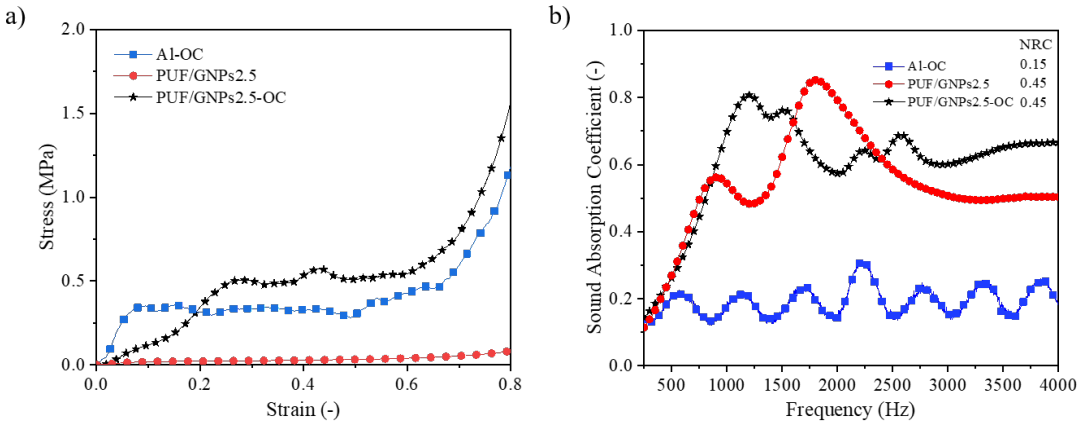

Figure 6. (**a**) Average stress–strain compressive curves; (**b**) sound absorption of Al-OC, PUF/GNPs2.5 and PUF/GNPs2.5-OC.

Table 4. Apparent density, stress peak, energy absorption, specific energy absorption, and thermal conductivity (n = 3).

Samples	Apparent Density ($kg \cdot m^{-3}$)		Stress Peak (MPa)		EAD ($MJ \cdot m^{-3}$) Strain: 0.8		SEA ($MJ \cdot m^{-3} \cdot kg^{-1}$) Strain: 0.8		Thermal Conductivity ($W \cdot m^{-1} \cdot K^{-1}$)	
	Mean Value	Std. Dev.	Mean Value	Std. Dev.	Mean Value	Std. Dev.	Mean Value	Std. Dev.	Mean Value	Std. Dev.
Al-OC	110	1.6	0.312	0.015	0.317	0.004	249	1.5	1.1781	0.0002
PUF/GNPs2.5	50	1.2	0.028	0.004	0.028	0.004	445	31	0.0355	0.0001
PUF/GNPs2.5-OC	116	6.4	0.396	0.005	0.401	0.002	127	8.8	0.0377	0.0001

Contrary to the hybrid structures composed by the Al-OC impregnated with dense polymers, epoxy [12] and polydimethylsiloxane [11], whose compressive mechanical behavior is governed by the dense materials, in this case it is the metal skeleton (Al-OC) that controls the compressive response under loading, as reported in a similar study describing the Al-OC filled with bacterial cellulose nanocomposite foam [15]. However, it should be noted that the weight of these structures is much lighter, and a good compromise between weight and strength can be achieved.

3.2.3. Sound Absorption

The sound absorption ability of the hybrid structure (evaluated by the sound absorption coefficient) present higher sound absorption values (peak at 1200 Hz with a value of 0.8 and followed by a nearly constant value of 0.7 for higher frequencies) (Figure 6b) when compared with the filling material. The increase of stiffness provided by the Al-OC structure can improve the absorption at low frequencies. Increased sound absorption can be obtained for thick specimens [55,56]. The NRC value for PUF/GNPs2.5-OC was 0.45, three times higher than for pristine Al-OC. These values are comparable with other cellular materials reported in the literature with similar thickness (around 22 mm) and density (120 kg/m^3) [57].

3.2.4. Thermal Conductivity

The values of thermal conductivity obtained for the hybrid PUF/GNPs2.5-OC are similar to those obtained for PUF and its nanocomposites, around 0.038 ($W \cdot m^{-1} \cdot K^{-1}$), suggesting that Al-OC contribution is negligible in the overall thermal conductivity value. This may be due to the small (about 1 mm) layer of filler foam (PUF and PUF/GNPs2.5) surrounding the metal foam that blocks the heat transfer. Another aspect is related to the highly porous structure of Al-OC, so the amount of solid material (Al-SiO3) that would effectively increase the conductivity value is very small. The same trend was observed in our previous works [11,12,15], in which the contribution of Al-OC was small regarding the filling materials. The polymer filler (e.g., polydimethylsiloxane [11], epoxy [12] and cellulose nanocomposites [15]) acts as an insulator, preventing effective heat transfer. On the other hand, some authors [58,59] have demonstrated that the open-cell metal foams can be used to enhance the low thermal conductivity of the pure phase change materials (PCM), composite PCMs and paraffin for application to many situations (e.g., latent heat thermal energy storage system, heat sink and heat exchanger). Furthermore, Fiedler et al. reported [60] that the polymeric adhesives exhibit a low thermal conductivity, and thus form thermal barriers between advanced pore morphology (APM) foam elements (sphere-like closed-cell aluminum foam), resulting a distinct decrease of the thermal conductivity of adhesively bonded APMs. Globally, hybrid PUF/GNPs2.5-OC can be used as a thermal insulation material [18,56].

4. Conclusions

In the present study, hybrid structures were prepared by impregnating an Al-OC foam with other cellular material, a PUF nanocomposite. Prior to the incorporation into the open structure of Al-OC foams, the standalone PUF nanocomposites were prepared with different amounts of GNPs and

GO and fully characterized. The presence of the carbon nanostructures in the PUF nanocomposites provided PUF with excellent fire retardancy, better mechanical strength, and thermal and acoustic insulating properties. The formulation with 2.5 wt% of GNPs was considered the more promising one. The process of filling the Al-OC open structure with the optimized PUF nanocomposite was successfully achieved, and the resulting hybrid structure maintain a low thermal conductivity value (0.038 $W \cdot m^{-1} \cdot K^{-1}$), high sound absorption coefficient specially at mid to high frequencies (NRC 0.45) and better mechanical behavior (the stress corresponding to 10% of deformation was improved in more than ten times). Therefore, these hybrid structures are thoroughly multifunctional materials with potential applications in the construction, automotive and, aeronautic sectors.

Supplementary Materials: The following are available online at http://www.mdpi.com/2075-4701/10/6/768/s1: Figure S1: Normalized FT-IR spectra of MDI, Polyol, PUF, PUF/GNPs2.5 and PUF/GO2.5; Figure S2: Flame response of PUF/GNPs1.0 and PUF/GO1.0; Figure S3: (a) Thermogravimetric (TG) and (b) derivative thermogravimetric (DTG) curves of PUF with different graphene based materials (GNPs and GO) additives under oxidative atmosphere; Figure S4: (a) EAD and (b) SEA curves of Al-OC; PUF/GNPs2.5 and PUF/GNPs2.5-OC.

Author Contributions: Conceptualization, S.C.P., P.A.A.P.M., I.D. and R.V.; methodology, S.C.P., I.D., P.A.A.P.M. and L.G.; formal analysis, S.C.P., I.D., P.A.A.P.M.; investigation, S.C.P., I.D., P.A.A.P.M., L.G. and R.V.; writing—original draft preparation, S.C.P. and P.A.A.P.M.; writing—review and editing, S.C.P., I.D., R.V. and P.A.A.P.M.; supervision, I.D.; P.A.A.P. and R.V. All authors have read and agreed to the published version of the manuscript.

Funding: This research was funded by Foundation for Science and Technology: UIDP/00481/2020-FCT and SFRH/BD/111515/2015, and Centro Portugal Regional Operational Program (Centro2020), under the PORTUGAL 2020 Partnership Agreement, through the European Regional Development Fund: CENTRO-01-0145-FEDER-022083.

Acknowledgments: This work was supported by the projects UIDB/00481/2020 and UIDP/00481/2020-FCT-Portuguese Foundation for Science and Technology and CENTRO-01-0145-FEDER-022083—Centro Portugal Regional Operational Programme (Centro2020), under the PORTUGAL 2020 Partnership Agreement, through the European Regional Development Fund and FCT scholarship grant SFRH/BD/111515/2015.

Conflicts of Interest: The authors declare no conflict of interest.

References

1. Zhao, C.Y.; Lu, W.; Tian, Y. Heat transfer enhancement for thermal energy storage using metal foams embedded within phase change materials (PCMs). *Sol. Energy* **2010**, *84*, 1402–1412. [CrossRef]
2. Chen, X.; Liang, Y.; Wan, L.; Xie, Z.; Easton, C.D.; Bourgeois, L.; Wang, Z.; Bao, Q.; Zhu, Y.; Tao, S.; et al. Construction of porous N-doped graphene layer for efficient oxygen reduction reaction. *Chem. Eng. Sci.* **2019**, *194*, 36–44. [CrossRef]
3. Ulker, Z.; Erkey, C. An emerging platform for drug delivery: Aerogel based systems. *J. Control. Release* **2014**, *177*, 51–63. [CrossRef] [PubMed]
4. Zhu, G.; Xu, H.; Dufresne, A.; Lin, N. High-adsorption, self-extinguishing, thermal, and acoustic-resistance aerogels based on organic and inorganic waste valorization from cellulose nanocrystals and red mud. *ACS Sustain. Chem. Eng.* **2018**, *6*, 7168–7180. [CrossRef]
5. Cao, J.; Wang, Z.; Yang, X.; Tu, J.; Wu, R.; Wang, W. Green synthesis of amphipathic graphene aerogel constructed by using the framework of polymer-surfactant complex for water remediation. *Appl. Surf. Sci.* **2018**, *444*, 399–406. [CrossRef]
6. Sing, K.S. Characterization of porous solids: An introductory survey. *Stud. Surf. Sci. Catal.* **1991**, *62*, 1–9. [CrossRef]
7. Wu, J.; Xu, F.; Li, S.; Ma, P.; Zhang, X.; Liu, Q.; Fu, R.; Wu, D. Porous Polymers as Multifunctional Material Platforms toward Task-Specific Applications. *Adv. Mater.* **2018**, *31*, 1802922. [CrossRef]
8. Ferreira, A.D.B.; Nóvoa, P.R.; Marques, A.T. Multifunctional material systems: A state-of-the-art review. *Compos. Struct.* **2016**, *151*, 3–35. [CrossRef]
9. Duarte, I.; Ferreira, J.M.F. Composite and Nanocomposite Metal Foams. *Materials* **2016**, *9*, 79. [CrossRef]
10. Duarte, I.; Vesenjak, M.; Krstulović-Opara, L.; Ren, Z. Crush performance of multifunctional hybrid foams based on an aluminium alloy open-cell foam skeleton. *Polym. Test.* **2018**, *67*, 246–256. [CrossRef]
11. Pinto, S.C.; Marques, P.A.; Vesenjak, M.; Vicente, R.; Godinho, L.; Krstulović-Opara, L.; Duarte, I. Characterization and physical properties of aluminium foam-polydimethylsiloxane nanocomposite hybrid structures. *Compos. Struct.* **2019**, *230*, 111521. [CrossRef]

12. Pinto, S.; Marques, P.A.; Vesenjak, M.; Vicente, R.; Godinho, L.; Krstulović-Opara, L.; Duarte, I. Mechanical, thermal, and acoustic properties of aluminum foams impregnated with epoxy/graphene oxide nanocomposites. *Metals* **2019**, *9*, 1214. [CrossRef]
13. Li, A.; Li, A.; He, S.; Xuan, P. Cyclic compression behavior and energy dissipation of aluminum foam–polyurethane interpenetrating phase composites. *Compos. Part A Appl. Sci. Manuf.* **2015**, *78*, 35–41. [CrossRef]
14. Reinfried, M.; Stephani, G.; Luthardt, F.; Adler, J.; John, M.; Krombholz, A. Hybrid foams—A new approach for multifunctional applications. *Adv. Eng. Mater.* **2011**, *13*, 1031–1036. [CrossRef]
15. Pinto, S.C.; Silva, N.H.; Pinto, R.J.; Freire, C.S.; Duarte, I.; Vicente, R.; Vesenjak, M.; Marques, P.A. Multifunctional hybrid structures made of open-cell aluminum foam impregnated with cellulose/graphene nanocomposites. *Carbohydr. Polym.* **2020**, *238*, 116197. [CrossRef]
16. Kausar, A. Polyurethane composite foams in high-performance applications: A review. *Polym. Technol. Eng.* **2017**, *57*, 346–369. [CrossRef]
17. Gama, N.V.; Silva, R.; Carvalho, A.; Ferreira, A.; Barros-Timmons, A. Sound absorption properties of polyurethane foams derived from crude glycerol and liquefied coffee grounds polyol. *Polym. Test.* **2017**, *62*, 13–22. [CrossRef]
18. Gama, N.V.; Soares, B.; Freire, C.S.; Silva, R.; Neto, C.P.; Barros-Timmons, A.; Ferreira, A. Bio-based polyurethane foams toward applications beyond thermal insulation. *Mater. Des.* **2015**, *76*, 77–85. [CrossRef]
19. Gama, N.V.; Silva, R.; Mohseni, F.; Davarpanah, A.; Amaral, V.S.; Ferreira, A.; Barros-Timmons, A. Enhancement of physical and reaction to fire properties of crude glycerol polyurethane foams filled with expanded graphite. *Polym. Test.* **2018**, *69*, 199–207. [CrossRef]
20. Xu, W.; Wang, G.; Zheng, X. Research on highly flame-retardant rigid PU foams by combination of nanostructured additives and phosphorus flame retardants. *Polym. Degrad. Stab.* **2015**, *111*, 142–150. [CrossRef]
21. Piszczyk, Ł.; Danowska, M.; Mietlarek-Kropidłowska, A.; Szyszka, M.; Strankowski, M. Synthesis and thermal studies of flexible polyurethane nanocomposite foams obtained using nanoclay modified with flame retardant compound. *J. Therm. Anal. Calorim.* **2014**, *118*, 901–909. [CrossRef]
22. Dong, Q.; Chen, K.; Jin, X.; Sun, S.; Tian, Y.; Wang, F.; Liu, P.; Yang, M. Investigation of flame retardant flexible polyurethane foams containing DOPO immobilized titanium dioxide nanoparticles. *Polymers* **2019**, *11*, 75. [CrossRef] [PubMed]
23. Nikje, M.M.A.; Moghaddam, S.T.; Noruzian, M. Preparation of novel magnetic polyurethane foam nanocomposites by using core-shell nanoparticles. *Polímeros* **2016**, *26*, 297–303. [CrossRef]
24. Huang, J.; Tang, Q.; Liao, W.; Wang, G.; Wei, W.; Li, C. Green preparation of expandable graphite and its application in flame-resistance polymer elastomer. *Ind. Eng. Chem. Res.* **2017**, *56*, 5253–5261. [CrossRef]
25. Pandey, G.; Thostenson, E.T. Carbon nanotube-based multifunctional polymer nanocomposites. *Polym. Rev.* **2012**, *52*, 355–416. [CrossRef]
26. Caglayan, C.; Gurkan, I.; Gungor, S.; Cebeci, H. The effect of CNT-reinforced polyurethane foam cores to flexural properties of sandwich composites. *Compos. Part A Appl. Sci. Manuf.* **2018**, *115*, 187–195. [CrossRef]
27. Colloca, M.; Gupta, N.; Porfiri, M. Tensile properties of carbon nanofiber reinforced multiscale syntactic foams. *Compos. Part B Eng.* **2013**, *44*, 584–591. [CrossRef]
28. Njuguna, J.; Pielichowski, K.; Desai, S. Nanofiller-reinforced polymer nanocomposites. *Polym. Adv. Technol.* **2008**, *19*, 947–959. [CrossRef]
29. Pinto, D.; Bernardo, L.; Amaro, A.; Lopes, S. Mechanical properties of epoxy nanocomposites using titanium dioxide as reinforcement—A review. *Constr. Build. Mater.* **2015**, *95*, 506–524. [CrossRef]
30. Cao, Z.-J.; Liao, W.; Wang, S.-X.; Zhao, H.-B.; Wang, Y.-Z. Polyurethane foams with functionalized graphene towards high fire-resistance, low smoke release, superior thermal insulation. *Chem. Eng. J.* **2019**, *361*, 1245–1254. [CrossRef]
31. Gharehbaghi, A.; Bashirzadeh, R.; Ahmadi, Z. Polyurethane flexible foam fire resisting by melamine and expandable graphite: Industrial approach. *J. Cell. Plast.* **2011**, *47*, 549–565. [CrossRef]
32. Yan, D.-X.; Xu, L.; Chen, C.; Tang, J.; Ji, X.; Li, Z. Enhanced mechanical and thermal properties of rigid polyurethane foam composites containing graphene nanosheets and carbon nanotubes. *Polym. Int.* **2012**, *61*, 1107–1114. [CrossRef]

33. Piszczyk, Ł.; Kosmela, P.; Strankowski, M. Elastic polyurethane foams containing graphene nanoplatelets. *Adv. Polym. Technol.* **2017**, *37*, 1625–1634. [CrossRef]
34. Kim, J.M.; Kim, H.; Kim, J.; Lee, J.W.; Kim, W.N. Effect of graphene on the sound damping properties of flexible polyurethane foams. *Macromol. Res.* **2017**, *25*, 190–196. [CrossRef]
35. Lee, J.; Jung, I. Tuning sound absorbing properties of open cell polyurethane foam by impregnating graphene oxide. *Appl. Acoust.* **2019**, *151*, 10–21. [CrossRef]
36. Silva, J. da Metodologias Experimentais Para a Determinação do Coeficiente de Absorção de Sonora em Materiais de Construção. Master's Thesis, University of Coimbra, Coimbra, Portugal, July 2008.
37. Colomer, J.-F.; Marega, R.; Traboulsi, H.; Meneghetti, M.; Van Tendeloo, G.; Bonifazi, D. Microwave-assisted bromination of double-walled carbon nanotubes. *Chem. Mater.* **2009**, *21*, 4747–4749. [CrossRef]
38. Cheng, Y.; Zhou, S.; Hu, P.; Zhao, G.; Li, Y.; Zhang, X.-H.; Han, W. Enhanced mechanical, thermal, and electric properties of graphene aerogels via supercritical ethanol drying and high-temperature thermal reduction. *Sci. Rep.* **2017**, *7*, 1439. [CrossRef]
39. Malucelli, G. The role of graphene in flame retardancy of polymeric materials: Recent advances. *Curr. Graphene Sci.* **2018**, *2*, 27–34. [CrossRef]
40. Idumah, C.I.; Hassan, A.; Affam, A.C. A review of recent developments in flammability of polymer nanocomposites. *Rev. Chem. Eng.* **2015**, *31*, 149–177. [CrossRef]
41. Sang, B.; Li, Z.; Li, X.-H.; Yu, L.-G.; Zhang, Z.-J. Graphene-based flame retardants: A review. *J. Mater. Sci.* **2016**, *51*, 8271–8295. [CrossRef]
42. Wang, Y.; He, Q.; Qu, H.; Zhang, X.; Zhu, J.; Zhao, G.; Lopera, H.C.; Yu, J.; Sun, L.; Bhana, S.; et al. Magnetic graphene oxide nanocomposites: Nanoparticles growth mechanism and property analysis. *J. Mater. Chem. C* **2014**, *2*, 9478–9488. [CrossRef]
43. Liu, H.; Dong, M.; Huang, W.; Gao, J.; Liu, Y.; Zheng, G.; Liu, C.; Shen, C.; Guo, Z. Lightweight conductive graphene/thermoplastic polyurethane foams with ultrahigh compressibility for piezoresistive sensing. *J. Mater. Chem. C* **2017**, *5*, 73–83. [CrossRef]
44. Gama, N.V.; Amaral, C.; Silva, T.; Vicente, R.; Coutinho, J.A.P.; Barros-Timmons, A.; Ferreira, A. Thermal energy storage and mechanical performance of crude glycerol polyurethane composite foams containing phase change materials and expandable graphite. *Materials* **2018**, *11*, 1896. [CrossRef] [PubMed]
45. Jawaid, M.; Bouhfid, R.; Qaiss, A.K. Functionalized graphene nanocomposites and their derivatives: Synthesis, processing and applications. In *Micro and Nano Technologies*; Elsevier Science: Amsterdam, The Nertherlands, 2018; ISBN 9780128145531.
46. Li, Y.; Zou, J.; Zhou, S.; Chen, Y.; Zou, H.; Liang, M.; Luo, W. Effect of expandable graphite particle size on the flame retardant, mechanical, and thermal properties of water-blown semi-rigid polyurethane foam. *J. Appl. Polym. Sci.* **2013**, *131*. [CrossRef]
47. Wang, G.; Fu, Y.; Guo, A.; Mei, T.; Wang, J.; Li, J.; Wang, X. Reduced graphene oxide—Polyurethane nanocomposite foam as a reusable photoreceiver for efficient solar steam generation. *Chem. Mater.* **2017**, *29*, 5629–5635. [CrossRef]
48. Najib, N.; Ariff, Z.M.; Bakar, A.; Sipaut, C. Correlation between the acoustic and dynamic mechanical properties of natural rubber foam: Effect of foaming temperature. *Mater. Des.* **2011**, *32*, 505–511. [CrossRef]
49. Arjunan, A.; Baroutaji, A.; Praveen, A.S.; Olabi, A.G.; Wang, C.J. Acoustic performance of metallic foams. In *Reference Module in Materials Science and Materials Engineering*; Elsevier BV: Amsterdam, The Netherlands, 2019.
50. Gwon, J.G.; Kim, S.K.; Kim, J.H. Sound absorption behavior of flexible polyurethane foams with distinct cellular structures. *Mater. Des.* **2016**, *89*, 448–454. [CrossRef]
51. Sung, G.; Kim, J.W.; Kim, J.H. Fabrication of polyurethane composite foams with magnesium hydroxide filler for improved sound absorption. *J. Ind. Eng. Chem.* **2016**, *44*, 99–104. [CrossRef]
52. Al-Ajlan, S.A. Measurements of thermal properties of insulation materials by using transient plane source technique. *Appl. Therm. Eng.* **2006**, *26*, 2184–2191. [CrossRef]
53. Jelle, B.P. Traditional, state-of-the-art and future thermal building insulation materials and solutions—Properties, requirements and possibilities. *Energy Build.* **2011**, *43*, 2549–2563. [CrossRef]
54. Vesenjak, M.; Krstulović-Opara, L.; Ren, Z. Characterization of irregular open-cell cellular structure with silicone pore filler. *Polym. Test.* **2013**, *32*, 1538–1544. [CrossRef]
55. Lu, T.J.; Hess, A.; Ashby, M.F. Sound absorption in metallic foams. *J. Appl. Phys.* **1999**, *85*, 7528–7539. [CrossRef]

56. *Handbook of Cellular Metals*; Degischer, H., Kriszt, B., Eds.; Wiley: Weinheim, Germany, 2002; ISBN 9783527303397.
57. Pedroso, M.; De Brito, J.; Silvestre, J. Characterization of eco-efficient acoustic insulation materials (traditional and innovative). *Constr. Build. Mater.* **2017**, *140*, 221–228. [CrossRef]
58. Xiao, X.; Zhang, P.; Li, M. Effective thermal conductivity of open-cell metal foams impregnated with pure paraffin for latent heat storage. *Int. J. Therm. Sci.* **2014**, *81*, 94–105. [CrossRef]
59. Li, W.; Qu, Z.; He, Y.; Tao, W. Experimental and numerical studies on melting phase change heat transfer in open-cell metallic foams filled with paraffin. *Appl. Therm. Eng.* **2012**, *37*. [CrossRef]
60. Fiedler, T.; Sulong, M.A.; Vesenjak, M.; Higa, Y.; Belova, I.V.; Öchsner, A.; Murch, G.E. Determination of the thermal conductivity of periodic APM foam models. *Int. J. Heat Mass Transf.* **2014**, *73*, 826–833. [CrossRef]